Assimilation of GPS Radio Occultation Data for an Intense Atmospheric River with the NCEP Regional GSI System

ZAIZHONG MA

State Key Laboratory of Numerical Modeling for Atmospheric Sciences and Geophysical Fluid Dynamics, Institute of Atmospheric Physics, Chinese Academy of Sciences, Beijing, China, and University Corporation for Atmospheric Research, Boulder, Colorado

YING-HWA KUO

University Corporation for Atmospheric Research, Boulder, Colorado

F. MARTIN RALPH, PAUL J. NEIMAN, GARY A. WICK, AND ELLEN SUKOVICH

NOAA/Earth System Research Laboratory/Physical Sciences Division, Boulder, Colorado

BIN WANG

State Key Laboratory of Numerical Modeling for Atmospheric Sciences and Geophysical Fluid Dynamics, Institute of Atmospheric Physics, Chinese Academy of Sciences, Beijing, China

(Manuscript received 12 January 2010, in final form 20 August 2010)

ABSTRACT

This paper uses a case study to explore the potential of Constellation Observing System for Meteorology, Ionosphere, and Climate (COSMIC) and Challenging Minisatellite Payload (CHAMP) global positioning system (GPS) radio occultation (RO) satellite data over the eastern Pacific Ocean to improve analyses and mesoscale forecasts of landfalling atmospheric rivers (ARs) along the U.S. West Coast. The case study is from early November 2006 and was a very high-impact event in the Pacific Northwest where it created torrential rainfall and severe flooding. Recent studies have shown that the COSMIC data offshore have the ability to better define the vertical and horizontal structure of the strong AR. This paper extends the earlier work by assessing the impact of assimilating the COSMIC data into the Advanced Research Weather Research and Forecasting (ARW-WRF) mesoscale numerical model (using a nested mode with 36-, 12-, and 4-km grid sizes) on a key 24-h forecast.

The data are assimilated using NCEP's Gridpoint Statistical Interpolation (GSI), and impacts are evaluated using Special Sensor Microwave Imager (SSM/I) satellite observations over the ocean and precipitation observations over land. The assimilation of GPS RO soundings made use of a local refractivity observation operator as well as an advanced nonlocal excess phase observation operator that considers the effects of atmospheric horizontal gradients. The results show that the assimilation of GPS RO soundings improved the moisture analysis for this AR event. This result supports conclusions from earlier observing systems simulation experiment (OSSE) studies, but in a real event. The use of a nonlocal excess phase observation operator can produce larger and more robust analysis increments. Although this is a single case study, the results are likely representative of the potential impacts of assimilating COSMIC data in other extreme AR and precipitation events and in other regions affected by landfalling ARs, for example, western Europe, western South America, and New Zealand.

1. Introduction

Water vapor is one of the most important variables of earth's atmosphere. Its distribution and transport play a crucial role in weather and climate. Atmospheric

Corresponding author address: Dr. Ying-Hwa Kuo, National Center for Atmospheric Research, Mesoscale and Microscale Meteorology Division, P.O. Box 3000, Boulder, CO 80307-3000.
E-mail: kuo@ucar.edu

DOI: 10.1175/2011MWR3342.1

rivers (ARs) are narrow (<~500 km wide) and long (>~2000 km) corridors of intense water vapor transport situated on the warm side of polar cold fronts. ARs over the eastern North Pacific Ocean often generate heavy orographic precipitation upon landfall, causing flooding events over the West Coast of the United States (Ralph et al. 2004, 2006; Neiman et al. 2008b). They can also play a significant role in transporting moisture from the tropical water vapor reservoir to the middle latitudes (e.g., Bao et al. 2006; Stohl et al. 2008).

Despite the importance of ARs to both weather and climate, their analysis and prediction remain a challenge for operational numerical weather prediction (NWP) partly because of the lack of traditional meteorological observations over the ocean. The optimal use of satellite data is crucial for improving the skills of NWP models. The integrated water vapor (IWV) observations gathered from Special Sensor Microwave Imager (SSM/I) (Hollinger et al. 1990) payloads aboard polar-orbiting satellites have proven crucial for monitoring these transient features over oceanic regions (Ralph et al. 2004, 2006; Neiman et al. 2008a,b). However, SSM/I observations contain no information on the vertical structure of moisture or winds associated with AR events. Passive microwave sounders provide some additional information on the vertical moisture distribution but only over very broad layers.

The atmospheric limb-sounding technique making use of radio signals transmitted by the global positioning system (GPS) satellites has emerged as a powerful and relatively inexpensive approach to sound the global atmosphere for temperature and water vapor (although not wind) in all weather conditions (Ware et al. 1996). As demonstrated by the proof-of-concept GPS Meteorology (GPS/MET) experiment, the Challenging Minisatellite Payload (CHAMP; Wickert et al. 2001) and the Satellite de Aplicaciones Cientificas-C (SAC-C; Hajj et al. 2004) missions, GPS radio occultation (RO) sounding data are shown to be of high accuracy and vertical resolution. With the launch of the joint U.S.–Taiwan Constellation Observing System for Meteorology, Ionosphere, and Climate/Formosa Satellite Mission 3 (COSMIC/FORMOSAT-3, hereafter COSMIC) mission in April 2006, GPS RO soundings have played an increasingly important role in weather prediction and climate monitoring (Anthes et al. 2008). Since August 2006, COSMIC has been providing ~2000 GPS RO profiles per day, uniformly distributed around the globe to support operational and research communities.

An important advancement in COSMIC is the use of a new open-loop tracking technique (Sokolovskiy et al. 2006), which allows about 90% of the soundings to reach to within 1 km of the surface (Anthes et al. 2008). As a result, COSMIC GPS RO soundings can be used to observe the structure in the otherwise data-sparse atmospheric boundary layer, providing valuable information on low-level atmospheric water vapor associated with an AR event (Neiman et al. 2008a; Wick et al. 2008). With uniform global coverage, GPS RO data are extremely valuable as inputs to operational NWP systems. Kuo et al. (2000) discussed various approaches to assimilate GPS RO soundings into weather prediction models. Recent studies have shown that the assimilation of GPS RO soundings has significant positive impact on the analysis and prediction of Hurricane Ernesto's genesis (H. Liu 2009, personal communication) and Typhoon Shanshan and mei-yu precipitation systems (Kuo et al. 2009). There have been very few studies of the impact of GPS RO data on the forecast skills associated with important precipitation systems such as an atmospheric river event.

In this study, we examine the impact of GPS RO soundings on an intense AR event formed over the eastern North Pacific Ocean that made landfall in the U.S. Pacific Northwest on 6–8 November 2006. Wick et al. (2008) compared integrated water vapor retrievals from SSM/I and COSMIC and showed that COSMIC GPS RO data can serve as an important new validation data source for SSM/I-derived products over the ocean; Neiman et al. (2008a) performed a detailed analysis of the water vapor structure associated with the 6–8 November AR event, using the moisture profiles retrieved from COSMIC GPS RO soundings that cut across the AR.

This paper serves as a sequel to these earlier studies listed above, with a focus on assessing the impacts of GPS RO soundings on the analysis and prediction of this high-impact AR event and its associated precipitation. The GPS impact experiment studies are performed with the National Centers for Environmental Prediction (NCEP) regional Gridpoint Statistical Interpolation (GSI) data-assimilation system (Wu et al. 2002) coupled with the Advanced Research Weather Research and Forecasting model (ARW-WRF; Skamarock et al. 2005). We also will make further comparison of local refractivity and nonlocal excess phase observation operators thatwere discussed in an observing system simulation experiment study (Ma et al. 2009).

This research contributes to the objectives of the Hydrometeorology Testbed (HMT; Ralph et al. 2005) by exploring the potential of a key new dataset—that is, GPS RO from COSMIC and CHAMP—and the use of new assimilation methods in the monitoring of conditions that contribute to the development of extreme precipitation events. The use of the ARW model to evaluate the impact of new satellite data on an important forecast challenge supports key goals of the Developmental Testbed Center (DTC; Bernardet et al. 2008). The focus on a flood-producing West Coast storm represents a unique

effort across two key test beds: one focused on a phenomenon (precipitation; HMT) and one focused on a key research and prediction tool (mesoscale modeling; DTC).

The paper is arranged as follows: section 2 provides the synoptic overview of the AR case in the early November 2006; section 3 discusses the configuration of the numerical model, the GPS RO observations, and our experiments; section 4 presents our analysis and forecast of this AR event; and section 5 offers the summary and conclusions.

2. Synoptic overview of the atmospheric river in early November 2006

The case studied in this paper is an intense AR event that took place over the eastern North Pacific Ocean in early November 2006. Neiman et al. (2008a) provided a detailed analysis of this event, using available satellite and other traditional observations. The 6–8 November 2006 AR event was ranked by Neiman et al. (2008a) as the first- or second-most intense AR storm among the 119 cases that occurred over the past nine years across the Pacific Northwest. Here, we provide only a brief description of this event. The 6–8 November AR event is well illustrated by SSM/I microwave images (Fig. 1), which show a narrow, well-defined plume of IWV extending northeastward from the tropical Pacific into the U.S. Pacific Northwest. Unlike most "Pineapple Express" cases, which last one day or so, the moist subtropical air in this event remained over the Pacific Northwest for 3–4 days. As a result, heavy rainfall occurred over the eastern Pacific Ocean and along the U.S. West Coast for a prolonged period, causing major flooding and damaging debris flows on 6–8 November 2006. According to Neiman et al. (2008a), numerous locations in northwestern Oregon and southwestern Washington reported more than 178 mm (about 7 inches) of precipitation in a single day (most of them on 6 November). Lees Camp in the Oregon Coast Range, a National Oceanic and Atmospheric Administration (NOAA) hourly rainfall station, recorded 363 mm (about 14.3 inches) of precipitation on 6 November, which broke Oregon's 24-h rainfall record. The distribution of precipitation is illustrated in Fig. 2. In summary, this intense atmospheric river event was characterized by an extended period of heavy rainfall that set records and, at some locations, exceeded 100-year precipitation thresholds for 24-h periods.

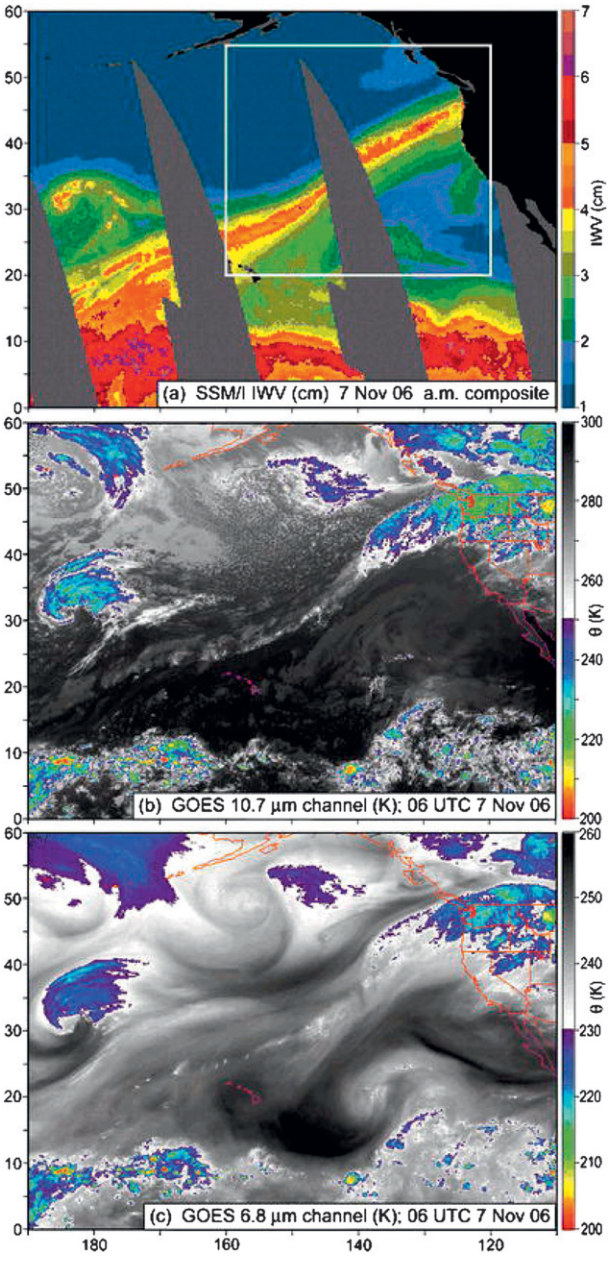

FIG. 1. Satellite imagery on the morning of 7 Nov 2006: (a) composite SSM/I image of IWV (cm) constructed from polar-orbiting swaths between ~0200 and 0615 UTC; (b) Geostationary Operational Environmental Satellite (GOES) 10.7-μm channel (i.e., infrared) image of surface and/or cloud-top brightness temperature (θ, K) at 0600 UTC; and (c) GOES 6.7-μm channel (i.e., water vapor) image of brightness temperature (θ, K) related to the moisture content of a broad layer of the upper troposphere [~(200–500 hPa)] at 0600 UTC. The white inset box in (a) is the coast domain shown in Fig. 3 (from Neiman et al. 2008a).

3. Numerical and observational aspects and experimental setup

a. The GSI/WRF data-assimilation and modeling system

In this paper, the assimilation of GPS data is performed with the NCEP regional GSI analysis system. The GSI system replaced the NCEP Spectral Statistical Interpolation analysis system (SSI; Parrish and Derber 1992) as the NCEP operational data-assimilation system in May 2007. The GSI has the advantage of incorporating locally

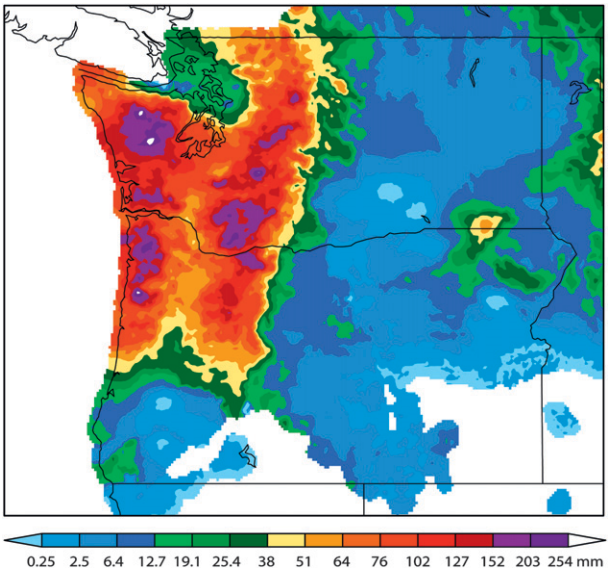

FIG. 2. The 24-h accumulative precipitation (mm) ending at 1200 UTC 7 Nov 2006 in domain D3 (see Fig. 3), based on gauge observations that are downscaled to a 4-km grid using a monthly precipitation climatology [i.e., Parameter-Elevation Regressions on Independent Slopes Model (PRISM); Daly et al. 1994].

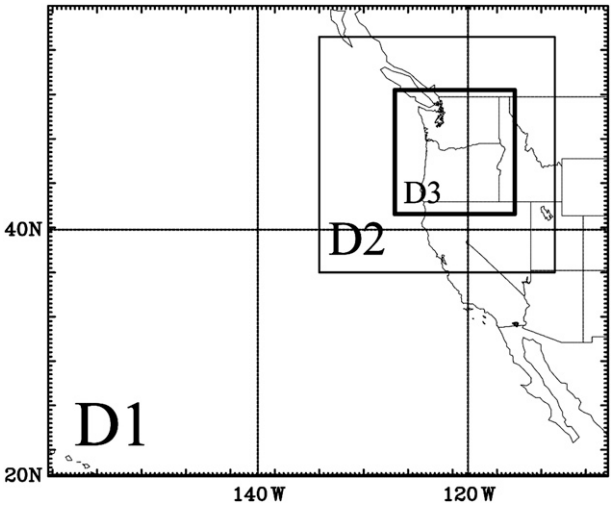

FIG. 3. Three nested domains used in the atmospheric river simulation experiment. Resolutions are 36, 12, and 4 km for domain 1 (D1), domain 2 (D2), and domain 3 (D3), respectively. The cycling assimilation experiment is performed on D1 and the 24-h WRF forecast is set up on D3, which only covers the northwest coast of the United States.

defined inhomogeneous anisotropic background errors. The GSI is an incremental three-dimensional variational (3D-Var) data-assimilation system. Its primary objective is to minimize the cost function, which measures the distance of an atmospheric field to the observations and the distance to the first guess. GSI can assimilate a wide range of conventional observations, satellite retrieval products, and satellite radiances data. With the use of the Community Radiative Transfer Model (CRTM), GSI can assimilate both clear and cloudy radiance data. In addition, the operational GSI system also assimilates the GPS RO data using the local refractivity observation operator (Cucurull et al. 2007).

The numerical model used in our study is the nonhydrostatic, triple-nested domain, mesoscale model WRF, which has been developed primarily at the National Center for Atmospheric Research. The model physics options include the Rapid Radiative Transfer Model (RRTM) longwave radiation, the Dudhia shortwave radiation scheme, the Yonsei University (YSU) PBL scheme, the Kain–Fritsch (new eta) scheme cumulus parameterization, and the new Thompson graupel microphysics scheme. Figure 3 shows the grid configuration used for the simulations. The grid's dimensions are 135 × 118, 160 × 160, and 259 × 259 in east–west and north–south directions in the 36-, 12-, and 4-km triple-nested domains, respectively. The assimilation was performed only on the coarse domain with 36-km resolution. There are 38 vertical eta levels, and the pressure at the top is 50 hPa.

b. GPS local and nonlocal operators

During an occultation event, the GPS receiver on board a low-earth orbit (LEO) satellite provides very accurate measurements of the phase and amplitude of radio signals transmitted by the GPS satellites. Based on these measurements, together with the knowledge of the occulting geometry (i.e., the precise positions and velocities of the GPS and LEO satellites), vertical profiles of ray bending angle are derived under the assumption of a spherically symmetric refractivity field. The atmospheric refractivity is then retrieved via the Abel transform (Phinney and Anderson 1968). Finally, the information on earth's atmosphere can be inferred from refractivity (N), which is a function of temperature (T; K), pressure (p; hPa), and water vapor pressure (e; hPa) after the ionospheric effect is removed in the neutral atmosphere (Smith and Weintraub 1953):

$$N = 77.6\frac{p}{T} + 3.73 \times 10^5 \frac{e}{T^2}. \quad (1)$$

A detailed description of GPS local refractivity (Cucurull et al. 2007) and the nonlocal excess phase (Sokolovskiy et al. 2005a; Liu et al. 2008; Ma et al. 2009) observation operators in the GSI system can be found in previous work, and thus only a brief review is provided here. The local refractivity operator is a simple and low-computational-cost approach to assimilate the GPS RO observations in a data-assimilation system. After the first-guess fields of temperature, pressure, and water

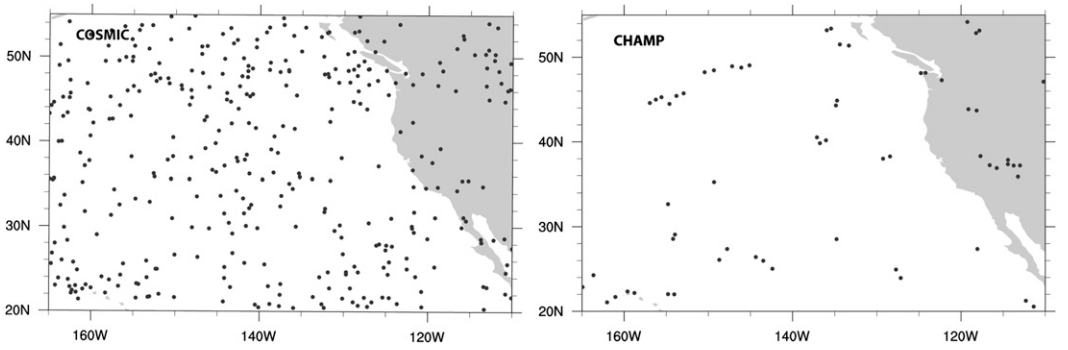

FIG. 4. The distribution of GPS RO soundings from (left) COSMIC and(right) CHAMP during the 1-week period from 0000 UTC 3 Nov to 1800 UTC 9 Nov 2006. There are 370 COSMIC and 63 CHAMP GPS RO soundings over the assimilation domain.

vapor on the model grid are interpolated to the RO observations' locations, the local refractivity is calculated based on Eq. (1). For the nonlocal excess phase operator, observed and modeled RO refractivities are integrated along a fixed ray path that does not depend on refractivity. Therefore, one can calculate a new observational ''variable,'' excess phase, with the nonlocal excess phase observation operator in the GSI system (Ma et al. 2009). Since the calculated local refractivity at the ray tangent point is a point value, and Abel-inverted GPS RO refractivity is a weighted average of the atmospheric refractivity along the ray path and above (Ahmad and Tyler 1998), significant errors could arise over regions with strong horizontal gradients of refractivity if the local refractivity operator is used to assimilate the GPS RO refractivity (Sokolovskiy et al. 2005b).

c. GPS RO observations

GPS RO soundings are obtained from the COSMIC Data Analysis and Archival Center (CDAAC) in Binary Universal Format for Data Representation (BUFR) format (www.cosmic.ucar.edu), which provides soundings of bending angle as a function of impact parameter, refractivity as a function of geometric height, and other derived atmospheric parameters as a function of the geometric height. The data also contain additional information related to the geometry of the radio occultation. In addition to COSMIC RO profiles, CHAMP RO profiles available for this case were also used in this study. The distribution of GPS RO soundings used in this AR case is shown in Fig. 4. The data are scattered geographically and homogeneously distributed over the entire model domain, with 370 soundings from COSMIC (Fig. 4a) and 63 from CHAMP (Fig. 4b) during the study period of 3–9 November 2006. COSMIC soundings are about 6 times as many as CHAMP. The total number of soundings available within a 3-h time window is shown in Fig. 5. We find that GPS soundings are not evenly distributed in time. In general, more data are available centered at around 0600 UTC. The main reason is that the COSMIC constellation of six satellites was still being deployed to their final orbits in November 2006. In addition to the CDAAC quality control (QC; Rocken et al. 2000; Kuo et al. 2004), all of the GPS RO observations used in this study also had to pass two additional QC procedures within the GSI data-assimilation system. One is the gross check, which is the standard QC for all types of observations being assimilated into the system; the other is that GPS RO observations are rejected if their deviation from forecast exceeds three standard deviations (Cucurull et al. 2007).

d. GPS impact experiment setup

To assess fully the impacts of GPS RO soundings on this intense AR event, two sets of experiments are conducted: First, a cycling assimilation experiment from 0000 UTC 3 November to 1800 UTC 9 November 2006, in which GSI is used for the analysis component and the WRF model is used for the 3-h forecast component.

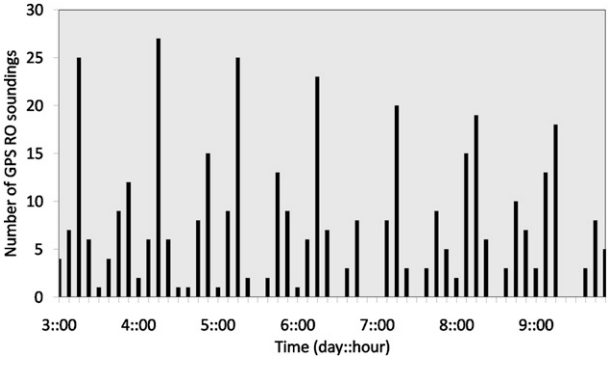

FIG. 5. The distribution of GPS RO soundings as a function of day and time (day:hour) in November 2006 in each 3-h assimilation window. There were no GPS RO soundings at 1200 UTC on 5–9 Nov and on 2100 UTC 6 Nov, 0000 UTC 7 Nov, and 0900 UTC 9 Nov.

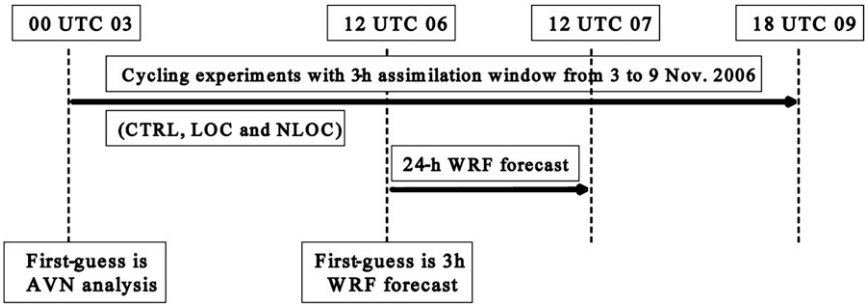

FIG. 6. The experiment design of assimilation cycling for 1 week (0000 UTC 3 Nov–1800 UTC 9 Nov 2006) and 24-h forecast starting 1200 UTC 06 Nov 2006.

Second, a 24-h forecast impact experiment starting 1200 UTC 6 November 2006 that is carried out with the WRF model. The experiment design is shown in Fig. 6.

Three experiments have been performed in each set:

1) The "CTRL" experiment that assimilates the same conventional and satellite measurements as used in the NCEP operations.
2) The "LOC" experiment is identical to the CTRL, except that GPS RO refractivity profiles are assimilated with the local refractivity observation operator.
3) The "NLOC" experiment is identical to the CTRL, except that GPS RO refractivity profiles are assimilated with the nonlocal excess phase observation operator.

All assimilation experiments are performed with continuous cycling with a 3-h assimilation window. For each cycling experiment, the first background fields are obtained from 3-h WRF forecasts initialized with NCEP aviation (AVN) analyses. However, the background fields in the subsequent cycling assimilation are the 3-h WRF forecast initialized with GSI analysis. Figure 5 shows the availability of GPS RO soundings within each 3-h window in the cycling experiment. The data volume at 0600 and 1800 UTC is always much larger than those at 0000 and 1200 UTC every day. We perform continuous assimilation up to one week, including a total of 56 analysis–update cycles. The CTRL, LOC, and NLOC experiments are performed with the same cycling assimilations, each with their own datasets, respectively. To evaluate the impact on forecasts, a 1-day forecast experiment is carried out with the 24-h-long forecast period starting at 1200 UTC 6 November 2006 (Fig. 6), after GSI assimilation is completed at that time.

4. Results

a. The 3-h cycling assimilation experiment

The impact of GPS RO data assimilation using a local refractivity operator with the global GSI system has been evaluated by Cucurull et al. (2007). In this study we mainly focus on examining the performance of the GPS nonlocal excess phase assimilation algorithm using the fractional difference $100\% \times (S_{\text{obs}} - S_{\text{mod}})/S_{\text{obs}}$, where S_{obs} and S_{mod} are the observed excess phase, and a corresponding model counterpart for NLOC. In general, the statistics of the observation minus background ($O - B$) and observation minus analysis ($O - A$) departure distributions provide useful diagnostic information on the effectiveness of assimilation (here O stands for GPS excess phase observation from nonlocal operator, and B and A are background and analysis projected in the space of observation). The $O - B$ departure represents the difference between the real observations and 3-h model prediction, which is used as the background. Figure 7 presents a comparison of the fractional differences between $O - B$ and $O - A$ in the 1-week cycling assimilation of refractivity profiles for the NLOC experiment. The statistics (Figs. 7a,b) are calculated for model levels below 5 km MSL from 3 to 9 November 2006. A total of 7353 observations were used during this period. Observation data at each level for each sounding are considered as one independent observation, so the number is much higher than the number of soundings. Figure 7a presents the fractional differences between the observations and model forecasts of excess phase. We note that the maximum and minimum departure varies from approximately −8.4% to 4.6%. Figure 7b is the fractional differences between the observation and the analysis. Obviously, Fig. 7b has smaller departure than $O - B$ (Fig. 7a), which is our expected result from 3D-Var data assimilation. The mean departure decreased about a factor of 3 from $O - B$ (−0.456) to $O - A$ (−0.105), while the standard deviation also reduces about 20% from $O - B$ (1.252) to $O - A$ (1.085). It is evident that the analysis fits the observations better after the assimilation procedure. The fact that the distance between the observation and analysis becomes smaller at the end of the minimization suggests a good behavior of the minimization algorithm in the 3D-Var GSI system.

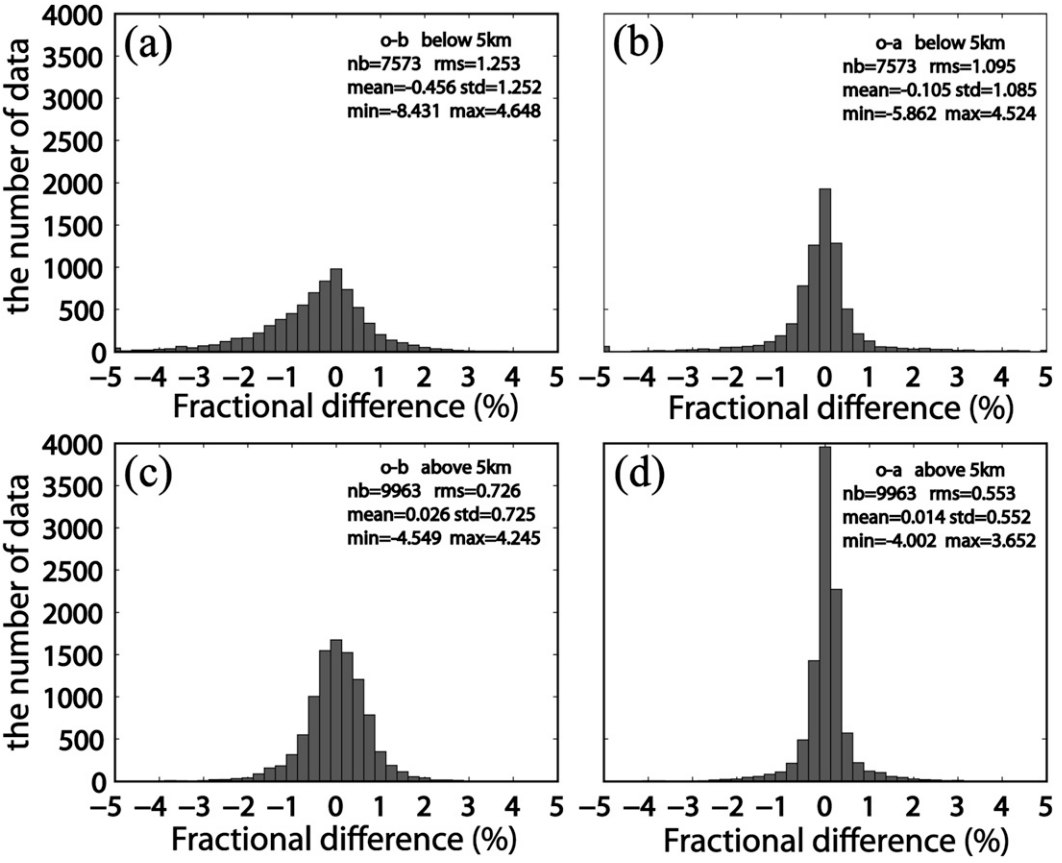

FIG. 7. The fractional difference (%) of excess phase departures [(a),(c) $O - B$ and (b),(d) $O - A$] in the nonlocal 1-week cycling assimilation experiment for impact heights (top) below 5 km and (bottom) above 5 km. Summary statistics are given in each panel.

The same statistics are also presented for altitudes above 5 km MSL (Figs. 7c,d). This allows us to examine the performance of GPS refractivity data assimilation in the GSI system at different height bins. Similarly, the statistics for above 5 km give good performance of GPS refractivity profiles data assimilation with nonlocal excess phase operator. Comparing with the behavior from a nonlocal operator below and above 5 km shown in Fig. 7, it is obvious that the larger improvements with a GPS nonlocal operator are in the lower troposphere (below 5 km). This suggests that the GPS RO provides the most useful information in the lower troposphere to improve the GSI analysis in this AR case study. Our explanation is that most of the water vapor is located in the lowest several kilometers of the troposphere. On the other hand, the model in general has poor performance in predicting the distribution of water vapor in the lower troposphere. The fact that $O - A$ is smaller than $O - B$ indicates that GPS RO refractivity observations have been assimilated successfully by the GSI system with nonlocal excess phase operator.

1) ASSIMILATION ANALYSIS AT 1200 UTC 6 NOVEMBER 2006

In this section, we choose the analysis at 1200 UTC 6 November 2006 to illustrate the influence of GPS RO profiles on the analysis and prediction of this event. This is the time that we choose to initialize the WRF model for 24-h forecast experiments with and without the assimilation of GPS RO data. This selected analysis is extracted from the 1-week cycling assimilation experiment starting from 0000 UTC 3 November 2006. Figure 8 shows the IWV at 1200 UTC 6 November 2006 derived from the model analysis with NLOC experiment. We also select this time period because it is close to the time of a key vertical cross-section analysis presented by Neiman et al. (2008a). Comparing with the SSM/I satellite image, the band of high IWV associated with the AR shown in the analysis is very similar to the SSM/I observation. This similarity is reflected in both the strength and range of IWV values associated with the atmospheric river.

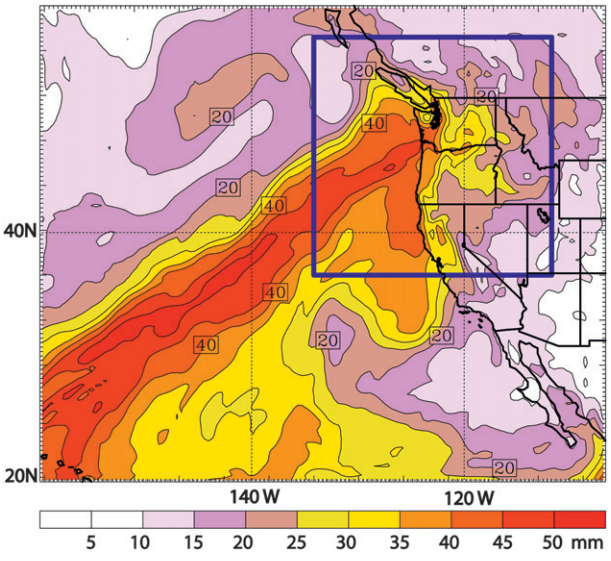

FIG. 8. Analysis of IWV (mm) in the cycling assimilation experiment when GPS RO soundings are assimilated with the nonlocal operator, valid at 1200 UTC 6 Nov 2006. The blue inset box represents the domain D2 in Fig. 3.

2) VERIFICATION OF 3-H FORECAST

The variational assimilation system performs a time–space adjustment of the model solution to all observations. The goal is to minimize a cost function penalizing the time–space misfits between the data and atmosphere fields, with the constraints of the model equations and their parameters. The basic analysis problem of the NCEP GSI system with the incremental approach is to minimize the cost function as follows (Wu et al. 2002):

$$J = \frac{1}{2}\mathbf{x}^{\mathrm{T}}\mathbf{B}^{-1}\mathbf{x} + \frac{1}{2}(H\mathbf{x} - \mathbf{y})^{\mathrm{T}}\mathbf{R}^{-1}(H\mathbf{x} - \mathbf{y}) = J_b + J_o, \tag{2}$$

where $\mathbf{x}$ is a vector of analysis increment; $\mathbf{B}$ is the background error covariance matrix; $\mathbf{y}$ is a vector of the observational residuals, that is, $\mathbf{y} = \mathbf{y}_{\mathrm{obs}} - H\mathbf{x}_{\mathrm{guess}}$; $\mathbf{R}$ is the observational and representativeness error covariance matrix; H is a transformation operator from the analysis variable to the form of the observation vector. Here J_b is the background term of cost function, and J_o is the observation term.

To conveniently evaluate the performance of GPS RO data assimilation, the observational term of the cost function in Eq. (2) is written as

$$J_o = J_{\mathrm{GPS}} + J_{\mathrm{others}}. \tag{3}$$

The observational residuals $\mathbf{y} = \mathbf{y}_{\mathrm{obs}} - H\mathbf{x}_{\mathrm{guess}}$ between observations and the modeled observations projected from first-guess field are called *innovations*. In this study, because of the 3-h forecast initialized by each 3D-Var analysis in the cycling, innovations can also be used to evaluate the performance of the 3-h model forecast after the assimilation of GPS RO data. Therefore, J_{GPS} here stands for the sum of departure between all GPS observations and 3-h forecast GPS soundings. All of the J_{GPS} in the cycling data-assimilation experiments are calculated to fit to observed refractivity N. Actually, J_{GPS} represents the sum of departures between all observed GPS soundings and forecasted values; this provides an assessment of the performance of GPS RO data assimilation.

A comparison of $J_{\mathrm{GPS}}(\mathbf{x})$ in terms of refractivity from CTRL, LOC, and NLOC experiments as a function of time is shown in Fig. 9. If we also look at Fig. 5 (the distribution of GPS sounding with time), we can see that the value of cost function of refractivity is larger when more GPS soundings are available. The value of cost function for LOC or NLOC is smaller than that of CTRL, when the cost function is above 1000 at the time of 0600 UTC for 3–7 November. We also want to compare the performance of GPS RO with the local and nonlocal operators. Figure 9 shows that NLOC has a smaller value of $J_{\mathrm{GPS}}(\mathbf{x})$, which means it fits better to the observed refractivity than LOC at most assimilation times. One may ask what causes the LOC and NLOC experiments to have different performance while they assimilate the same data with the same data-assimilation system. The only difference between these two experiments is the different observation operators used for the assimilation of GPS RO refractivity data. Obviously, there are many GPS RO soundings located in and around the AR in every assimilation cycle, where there are significant horizontal moisture gradients. Theoretically, the simple local refractivity operator cannot properly account for the effects of strong horizontal gradients, while the nonlocal excess phase operator is a two-dimensional operator that is capable of taking into account the along-track refractivity horizontal gradients. This provides an explanation for the superior performance of the nonlocal excess phase operator.

To gain insights into the impact of GPS RO data assimilation, we show in Figs. 10a,b the vertical profiles of the bias and standard deviation errors of 3-h WRF forecasts (which serve as the ''background'' for the data assimilation) verified against GPS RO refractivity (units: N) observations within ±1.5 h. The vertical distribution of GPS data points assimilated during the 1-week cycling experiment is shown in Fig. 10c. It is clear that both the bias and standard deviation errors of LOC and NLOC with GPS RO data are smaller than CTRL at most model levels, especially below ~4 km MSL. The

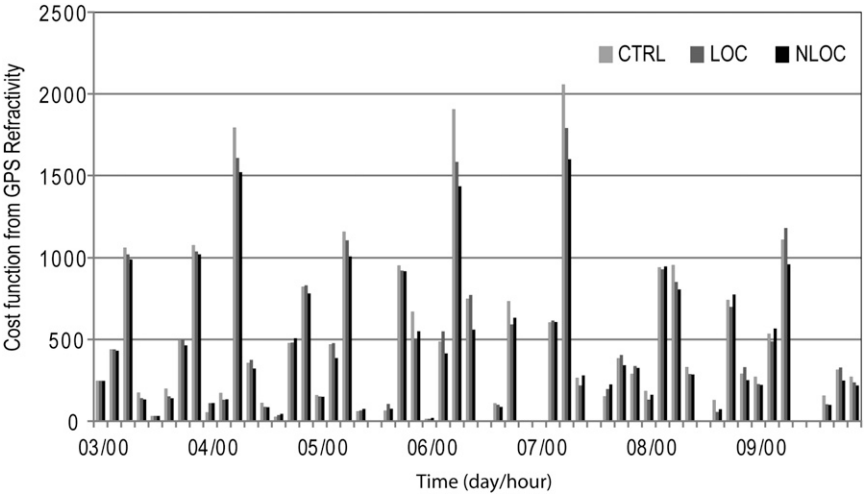

FIG. 9. The 3-h WRF forecasts fit to GPS refractivity as a function of day and time (day/hour, November 2006) in the cycling experiments. The values are cost function for CTRL (dark gray line), LOC (light gray line), and NLOC (black line) runs.

fact that 3-h forecasts based on analyses with the assimilation of GPS RO data verified better with the observations indicates that these analyses are improved with the assimilation of the GPS RO data (with either local or nonlocal observation operators). For example, the GPS RO measurements reduce a negative bias in the layer between 2 and ~4 km for LOC and NLOC. A closer look shows that NLOC has a superior performance (more accurate 3-h forecast), particularly in terms of standard deviation error, to the LOC experiment below ~4 km. Again, this supports the conclusion that the use of a nonlocal excess phase observation operator can assimilate the GPS RO data more effectively for this atmospheric river event, which has with significant horizontal gradients of water vapor as documented by SSM/I data (Fig. 1).

b. *The 24-h forecast impact experiment*

In this atmospheric river event, an intense storm ultimately made landfall across the U.S. Pacific Northwest, mainly in Washington and Oregon, on 6–8 November

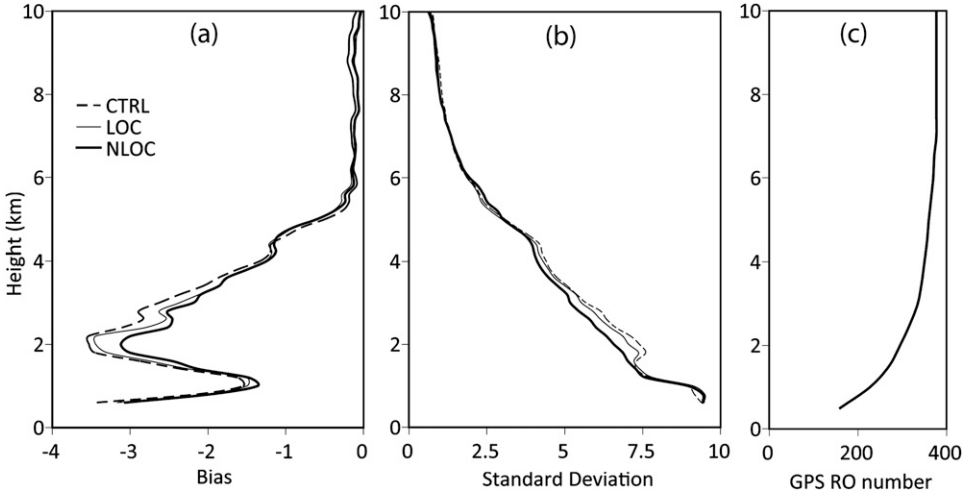

FIG. 10. Vertical profiles of statistics in the cycling experiments domain from 0000 UTC 3 Nov to 1800 UTC 9 Nov 2006. (a) Bias and (b) standard deviation errors of 3-h WRF forecasts verified against GPS RO refractivity (unit: N) with the height (km) for CTRL (dashed curve), LOC (thin curve), and NLOC (thick curve). (c) The total number of verifying GPS soundings at each level during the 1-week cycling period.

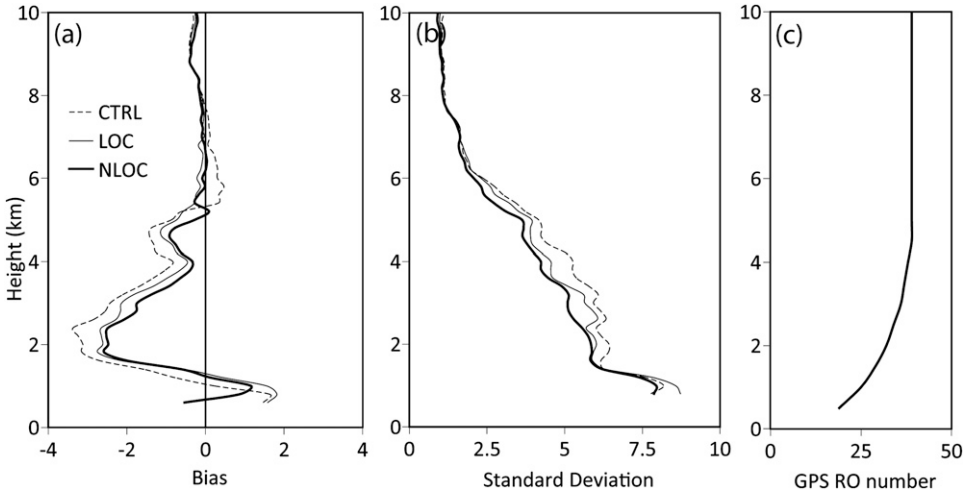

FIG. 11. Verification of the 24-h forecast with–without assimilating GPS RO data starting at 12 UTC 6 Nov 2006. (a) Bias and (b) standard deviation errors of the 24-h forecast fields fit to refractivity (unit: N) with the height (km) for CTRL (dashed curve), LOC (thin curve), and NLOC (thick curve). (c) The total number of verifying GPS soundings at each level during 24-h forecast period.

2006. To further evaluate the GPS RO observation impact on forecasting this extreme rainfall event, we performed a 24-h forecast with 4-km resolution over the innermost domain (see Fig. 3) starting at 1200 UTC 6 November.

1) VERIFICATION WITH GPS REFRACTIVITY

As the verification of the 3-h forecast in the cycling experiments, we performed the same verification with GPS refractivity observations for these 24-h forecast

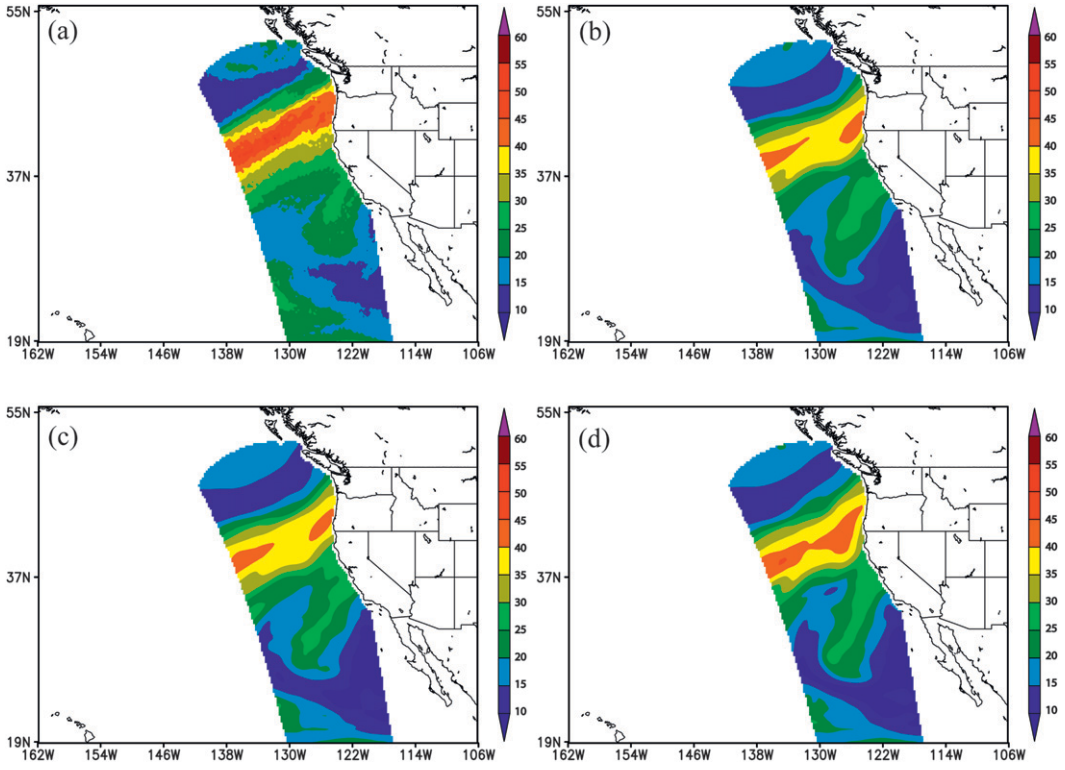

FIG. 12. Verification of the forecast with SSM/I IWV observations (mm) validated at 0200 UTC 7 Nov 2006. (a) SSM/I IWV; and forecasted IWV based on (b) CTRL, (c) LOC, and (d) NLOC experiments.

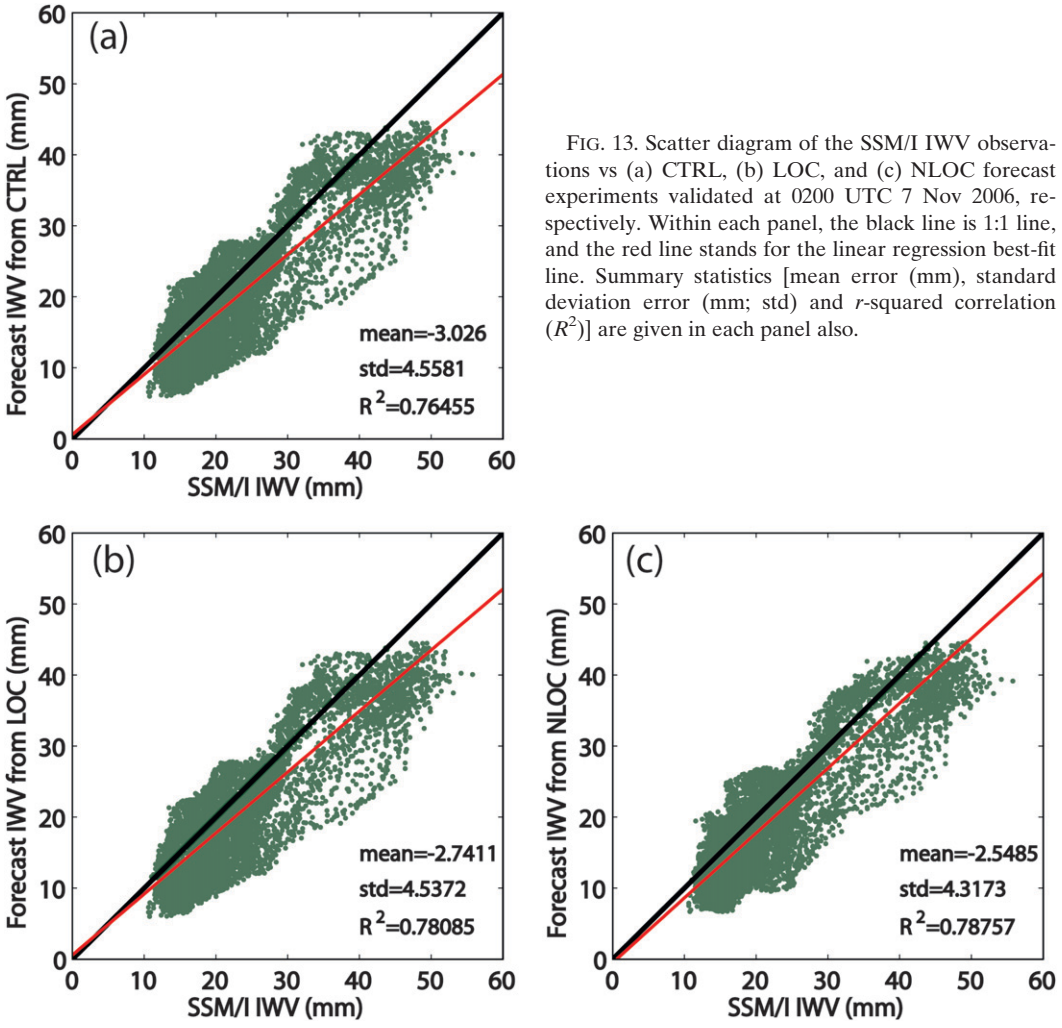

FIG. 13. Scatter diagram of the SSM/I IWV observations vs (a) CTRL, (b) LOC, and (c) NLOC forecast experiments validated at 0200 UTC 7 Nov 2006, respectively. Within each panel, the black line is 1:1 line, and the red line stands for the linear regression best-fit line. Summary statistics [mean error (mm), standard deviation error (mm; std) and *r*-squared correlation (R^2)] are given in each panel also.

experiments in the coarse domain (D1 shown in Fig. 3). To be more accurate, we compare the forecast with GPS observations within ±0.5 h. Similar to the verification of 3-h forecast discussed earlier, we find that the assimilation of GPS RO data improves the forecast and the nonlocal excess phase observation operator performs better than the local refractivity observation operator (Fig. 11). More importantly, the statistics results for the 24-h forecast verified against GPS refractivity are better than the 3-h forecast in the cycling assimilation experiment.

2) VERIFICATION WITH SSM/I

Besides GPS refractivity, the SSM/I IWV data are also used to evaluate the results of the 24-h forecast in this AR case study. The SSM/I IWV retrieval algorithm used in this case was the Wentz Optimal Statistical algorithm (Wentz 1995), which gives one of the best overall agreement with the COSMIC IWV (Wick et al. 2008). The SSM/I data are not assimilated and thus provide an independent source for validation.

Figure 12 shows the comparison of SSM/I IWV and model forecasts from the three experiments (CTRL, LOC, and NLOC) valid at 0200 UTC 7 November 2006 (14-h forecast). The results clearly show the forecast that assimilated GPS RO data with the NLOC method most accurately depicted the large IWV content within the AR. The mean and standard deviation errors (mm) can be reduced with GPS RO data (shown in Fig. 13), at least for this forecast time. To investigate the forecast performance with GPS data, verification statistics were calculated using 8 SSM/I swaths during the 24-h forecast time period (see Table 1). All the model experiments show negative IWV bias. We also found that the largest negative bias occurred in the high IWV regions. The maximum IWV in the 36-km WRF model tops out at

TABLE 1. Comparison of (forecast − observed) statistics among the three forecast experiments. The mean and standard deviation errors of IWV (mm) are shown as the function of forecast time (day in November/hour), when the 24-h duration forecast experiments are verified with the SSM/I IWV observations.

Mean FCST	6/15 3 h	6/16 4 h	6/17 5 h	6/18 6 h	7/02 14 h	7/03 15 h	7/04 16 h	7/05 17 h	Avg
CTRL	−1.52	−2.31	−1.37	−2.83	−3.03	−2.37	−3.11	−1.79	−2.29
LOC	−1.48	−2.43	−1.54	−2.97	−2.74	−2.11	−3.06	−1.76	−2.26
NLOC	−1.63	−2.28	−1.38	−2.76	−2.55	−1.92	−2.91	−1.71	−2.14
Standard deviation FCST	6/15 3 h	6/16 4 h	6/17 5 h	6/18 6 h	7/02 14 h	7/03 15 h	7/04 16 h	7/05 17 h	Avg
CTRL	3.9	3.39	3.31	3.49	4.56	4.43	4.05	3.34	3.81
LOC	4.1	3.38	3.39	3.47	4.54	4.32	4.01	3.55	3.85
NLOC	4.0	3.30	3.27	3.32	4.32	4.21	3.78	3.41	3.71

45 mm, while SSM/I exceeds 55 mm. The limiting factor in this case is the horizontal resolution of the 36-km model grid for domain D1, which simply cannot resolve the large IWV amount. Repeating the experiments at 12- or 4-km will likely reduce the negative biases. The average mean error is reduced from −2.29 mm (CTRL) to −2.26 mm (LOC) and −2.14 mm (NLOC). For standard deviation errors, LOC (3.85 mm) is slightly worse than the CTRL (3.81 mm), while the performance from NLOC (3.71 mm) improves. We also noted that there is significant time variation of the mean bias statistics. It varies from −1.37 to −3.11 mm for CTRL (a factor of 2.27) and LOC from −1.48 to 3.06 mm (a factor of 2.07), while NLOC is slightly more stable (i.e., a factor of 2.00). The ''timing'' and ''location'' of the predicted AR might have accounted for these variations.

COSMIC has a clear positive impact when the nonlocal observation operator is used. The impact of COSMIC is not as obvious with the local observation operator. This is by far the most robust evaluation of the nonlocal observation operator to date. It is the first case study documentation showing that the nonlocal operator works in an environment with significant horizontal gradients of refractivity (e.g., due to moisture distributions) and that it performs better than the local operator under these conditions. In theory, the local operator does not model GPS RO observables as well when there are significant horizontal gradients. Atmospheric river conditions represent an ideal situation in which to evaluate this, because ARs contain significant refractivity gradients due to moisture variations (Ralph et al. 2004).

To investigate further, we now compare the impact on the initial fields of the 1-day forecast experiment with the assimilation of GPS RO data, using local and nonlocal observation operators. As in Fig. 8, but for a zoomed-in domain D2, Fig. 14a shows the analysis of IWV in the cycling assimilation experiment when GPS RO soundings are assimilated with the nonlocal operator valid at 1200 UTC 6 November 2006. The difference field in IWV between the CTRL and LOC is presented in Fig. 14b, and

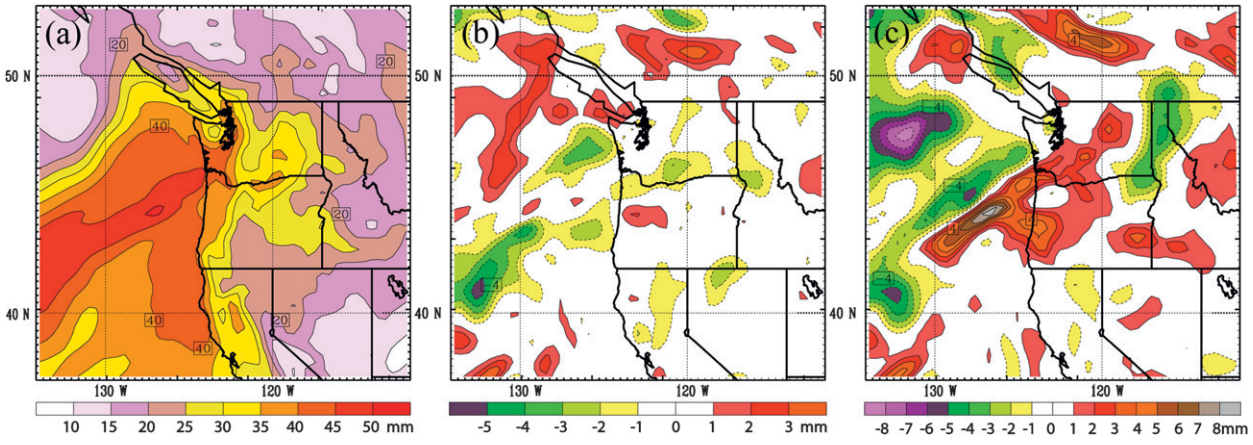

FIG. 14. (a) Analysis of IWV (mm; domain D2 in Fig. 3) in the cycling assimilation experiment at 1200 UTC 6 Nov 2006, when GPS RO soundings are assimilated with nonlocal operator. Difference fields of IWV (mm) in the cycling assimilation experiments at 1200 UTC 6 Nov 2006: (b) LOC − CTRL; and (c) NLOC − CTRL.

the difference between CTRL and NLOC in Fig. 14c. From the difference fields, we can see that the impacts of GPS RO data assimilation on this event are most prominent in the vicinity of the AR using either the local or nonlocal operator to assimilate the GPS RO soundings, even though the distribution of GPS RO soundings are relatively uniform over the assimilation domain in the cycling experiments (as shown in Fig. 5). Another noticeable result is that the NLOC experiment produces larger changes (both in terms of the amount and area) than the LOC (comparing Fig. 14b with Fig. 14c). It is interesting to note that the sign also changes at some locations and that the pattern shift looks much like what would be expected from shifting the position of a long, narrow filament of IWV, that is, the AR. The mean absolute impact of NLOC is larger than LOC, which is consistent with results from observing systems simulation experiments (OSSEs) (Ma et al. 2009). It is encouraging that the real data experiments give a similar conclusion, that is, that the nonlocal operator with the assimilation of excess phase produces more significant changes on the moisture analysis than the simple refractivity operator, especially over the region of the AR where there are strong water vapor gradients.

5. Summary and discussion

The impact of GPS RO profiles on an intense atmospheric river case has been evaluated with both local refractivity and nonlocal excess phase operators in the GSI/WRF system. In the cycling assimilation experiment, three experiments (CTRL, LOC, and NLOC) were conducted to examine the performance with the GPS RO profiles data assimilation on this storm from 3 to 9 November 2006. Since this intense AR event took place mainly over the data-sparse eastern North Pacific Ocean, GPS RO soundings, especially the near-real-time COSMIC data that provide the important new dataset, significantly increased the observational information. The results in the cycling assimilation and 24-h forecast experiments demonstrate the potential of GPS RO data, as a new type of satellite observation, to improve the analysis and prediction of an AR event.

The feasibility of GPS RO soundings data assimilation in the NCEP GSI system is tested with the advanced nonlocal excess phase operator in this atmospheric river case. Through comparison with the simple local refractivity operator, the nonlocal excess phase operator shows clear advantage in its ability to more accurately model the GPS RO data, which produces greater accuracy in an environment with strong horizontal water vapor and temperature gradients in the vicinity of the AR, but without more significant computational cost. It also provides further proof to support the conclusions drawn from the related OSSE experiment by Ma et al. (2009).

This study has demonstrated the potential benefits of GPS RO data on numerical simulations of an intense atmospheric river with the GSI system. Research regarding the impact assessment of a GPS nonlocal excess phase operator in the NCEP GSI system with a real case is an important step toward its operational application.

Future work on this subject is being planned as part of the broader objectives of HMT and contributes to the demonstration of new data and methods to the analysis of conditions that contribute to the development of extreme precipitation. It is recommended that additional cases are studied, which would allow an assessment of the representativeness of this case study result to other high-impact events along the U.S. West Coast, and that it be extended to include assessments of quantitative precipitation forecast skill using methods for extreme precipitation developed recently (Ralph et al. 2010). This could be carried out in coordination with a joint research effort on extreme quantitative precipitation forecast (QPF) between HMT and DTC that is now under way.

Acknowledgments. We want to acknowledge Louis Uccellini, Steve Lord, Greg Holland, Jim Yoe, and John LeMarshall for their support and encouragement of this work; Wan-Shu Wu, John Derber, Lidia Cucurull, and Russ Treadon for many fruitful discussions; and Xiaoyan Zhang (NCAR) for her comments and suggestions regarding an initial manuscript. This work is supported by the NCAR ASP Graduate Visitor Program, NCAR/MMM, NCEP/EMC and JCSDA, and NSF under corporate agreements with UCAR Awards ATM-0410018 and INT-0129369, and the National Aeronautics and Space Administration under Grant NNX08AI23G.

REFERENCES

Ahmad, B., and G. L. Tyler, 1998: The two-dimensional resolution kernel associated with retrieval of ionospheric and atmospheric refractivity profiles by Abelian inversion of radio occultation phase data. *Radio Sci.,* **33,** 129–142.

Anthes, R. A., and Coauthors, 2008: The COSMIC/FORMOSAT-3 mission: Early results. *Bull. Amer. Meteor. Soc.,* **89,** 313–333.

Bao, J.-W., S. A. Michelson, P. J. Neiman, F. M. Ralph, and J. M. Wilczak, 2006: Interpretation of enhanced integrated water-vapor bands associated with extratropical cyclones: Their formation and connection to tropical moisture. *Mon. Wea. Rev.,* **134,** 1063–1080.

Bernardet, L., and Coauthors, 2008: The Developmental Testbed Center and its winter forecasting experiment. *Bull. Amer. Meteor. Soc.,* **89,** 611–627.

Cucurull, L., L. C. Derber, R. Treadon, and R. J. Purser, 2007: Assimilation of global positioning system radio occultation

observations into NCEP's Global Data Assimilation System. *Mon. Wea. Rev.,* **135,** 3174–3193.

Daly, C., R. P. Neilson, and D. L. Phillips, 1994: A statistical-topographic model for mapping climatological precipitation over mountainous terrain. *J. Appl. Meteor.,* **33,** 140–158.

Hajj, G. A., and Coauthors, 2004: CHAMP and SAC-C atmospheric occultation results and intercomparisons. *J. Geophys. Res.,* **109,** D06109, doi:10.1029/2003JD003909.

Hollinger, J. P., J. L. Perirce, and G. A. Poe, 1990: SSM/I instrument evaluation. *IEEE Trans. Geosci. Remote Sens.,* **28,** 781–790.

Kuo, Y.-H., S. V. Sokolovskiy, R. A. Anthes, and F. Vandenberghe, 2000: Assimilation of GPS radio occultation data for numerical weather prediction. *Terr. Atmos. Ocean. Sci.,* **11,** 157–186.

——, T.-K. Wee, S. Sokolovskiy, C. Rocken, W. Schreiner, D. Hunt, and R. A. Anthes, 2004: Inversion and error estimation of GPS radio occultation data. *J. Meteor. Soc. Japan,* **82,** 507–531.

——, H. Liu, Y.-R. Guo, C.-T. Terng, and Y.-T. Lin, 2009: Impact of FORMOSAT-3/COSMIC data on typhoon and mei-yu prediction. *Recent Progress in Atmospheric Sciences: Applications to the Asia-Pacific Region,* K.-N. Liou and M.-D. Chou, Eds., World Scientific, 458–483.

Liu, H., J. L. Anderson, Y. H. Kuo, C. Snyder, and A. Caya, 2008: Evaluation of a nonlocal quasi-phase observation operator in assimilation of CHAMP radio occultation refractivity with WRF. *Mon. Wea. Rev.,* **136,** 242–256.

Ma, Z., Y.-H. Kuo, B. Wang, W.-S. Wu, and S. Sokolovskiy, 2009: Comparison of local and nonlocal observation operators for the assimilation of GPS RO data with the NCEP GSI system: An OSSE study. *Mon. Wea. Rev.,* **137,** 3575–3587.

Neiman, P. J., F. M. Ralph, G. A. Wick, Y.-H. Kuo, T.-K. Wee, Z. Ma, G. H. Taylor, and M. D. Dettinger, 2008a: Diagnosis of an intense atmospheric river impacting the Pacific Northwest: Storm summary and offshore vertical structure observed with COSMIC satellite retrievals. *Mon. Wea. Rev.,* **136,** 4398–4420.

——, ——, ——, J. Lundquist, and M. D. Dettinger, 2008b: Meteorological characteristics and overland precipitation impacts of atmospheric rivers affecting the West Coast of North America based on eight years of SSM/I satellite observations. *J. Hydrometeor.,* **9,** 22–47.

Parrish, D. F., and J. C. Derber, 1992: The National Meteorological Center's spectral statistical-interpolation analysis system. *Mon. Wea. Rev.,* **120,** 1747–1763.

Phinney, R. A., and D. L. Anderson, 1968: On the radio occultation method for studying planetary atmospheres. *J. Geophys. Res.,* **73** (5), 1819–1827.

Ralph, F. M., P. J. Neiman, and G. A. Wick, 2004: Satellite and CALJET aircraft observations of atmospheric rivers over the eastern North Pacific Ocean during the winter of 1997/98. *Mon. Wea. Rev.,* **132,** 1721–1745.

——, and Coauthors, 2005: Improving short-term (0–48 hour) cool-season quantitative precipitation forecasting: Recommendations from a USWRP workshop. *Bull. Amer. Meteor. Soc.,* **86,** 1619–1632.

——, P. J. Neiman, G. A. Wick, S. I. Gutman, M. D. Dettinger, D. R. Cayan, and A. B. White, 2006: Flooding on California's Russian River: Role of atmospheric rivers. *Geophys. Res. Lett.,* **33,** L13801, doi:10.1029/2006GL026689.

——, E. Sukovich, D. Reynolds, M. Dettinger, S. Weagle, W. Clark, and P. J. Neiman, 2010: Assessment of extreme quantitative precipitation forecasts and development of regional extreme event thresholds using data from HMT-2006 and COOP observers. *J. Hydrometeor.,* **11,** 1286–1304.

Rocken, C., Y. H. Kuo, W. S. Schreiner, D. Hunt, S. Sokolovskiy, and C. McCormick, 2000: COSMIC system description. *Terr. Atmos. Ocean. Sci.,* **11,** 21–52.

Skamarock, W. C., J. B. Klemp, J. Dudhia, D. O. Gill, D. M. Barker, W. Wang, and J. G. Powers, 2005: A description of the advanced research WRF version 2. NCAR Tech. Note NCAR/TN-468+STR, 100 pp.

Smith, E. K., and S. Weintraub, 1953: The constants in the equation for atmospheric refractivity index at radio frequencies. *Proc. IRE,* **41,** 1035–1037.

Sokolovskiy, S., Y. H. Kuo, and W. Wang, 2005a: Assessing the accuracy of a linearized observation operator for assimilation of the Abel-retrieved refractivity: Case simulation with high-resolution weather model. *Mon. Wea. Rev.,* **133,** 2200–2212.

——, ——, and ——, 2005b: Evaluation of a linear phase observation operator with CHAMP radio occultation data and high-resolution regional analysis. *Mon. Wea. Rev.,* **133,** 3053–3059.

——, Y.-H. Kuo, C. Rocken, W. S. Schreiner, D. Hunt, and R. A. Anthes, 2006: Monitoring the atmospheric boundary layer by GPS radio occultation signals recorded in the open-loop mode. *Geophys. Res. Lett.,* **33,** L12813, doi:10.1029/2006GL025955.

Stohl, A., C. Forster, and H. Sodemann, 2008: Remote sources of water vapor forming precipitation on the Norwegian west coast at 60°N—A tale of hurricanes and an atmospheric river. *J. Geophys. Res.,* **113,** D05102, doi:10.1029/2007JD009006.

Ware, M., and Coauthors, 1996: GPS sounding of the atmosphere from low earth orbit: Preliminary results. *Bull. Amer. Meteor. Soc.,* **77,** 19–40.

Wentz, F. J., 1995: The intercomparison of 53 SSM/I water vapor algorithms. Remote Sensing Systems Tech. Rep., 19 pp.

Wickert, J., and Coauthors, 2001: Atmosphere sounding by GPS radio occultation: First results from CHAMP. *Geophys. Res. Lett.,* **28** (17), 3263–3266.

Wick, G. A., Y.-H. Kuo, F. M. Ralph, T.-K. Wee, and P. J. Neiman, 2008: Intercomparison of integrated water vapor retrievals from SSM/I and COSMIC. *Geophys. Res. Lett.,* **35,** L21805, doi:10.1029/2008GL035126.

Wu, W.-S., R. J. Purser, and D. F. Parrish, 2002: Three-dimensional variational analysis with spatially inhomogeneous covariances. *Mon. Wea. Rev.,* **130,** 2905–2916.